# SCIENTIFIC REPORTS

OPEN

In vivo evaluation of radiotracers targeting the melanin-concentrating hormone receptor 1: [^{11}C]SNAP-7941 and [^{18}F]FE@SNAP reveal specific uptake in the ventricular system

Markus Zeilinger[1,2], Monika Dumanic[1], Florian Pichler[1,2], Lubos Budinsky[3], Wolfgang Wadsak [1,4,5], Katharina Pallitsch[6], Helmut Spreitzer[7], Rupert Lanzenberger[8], Marcus Hacker[1], Markus Mitterhauser[1,9,10] & Cécile Philippe[1,9]

The MCHR1 is involved in the regulation of energy homeostasis and changes of the expression are linked to a variety of associated diseases, such as diabetes and adiposity. The study aimed at the *in vitro* and *in vivo* evaluation of [^{11}C]SNAP-7941 and [^{18}F]FE@SNAP as potential PET-tracers for the MCHR1. Competitive binding studies with non-radioactive derivatives and small-animal PET/CT and MRI brain studies were performed under baseline conditions and tracer displacement with the unlabelled MCHR1 antagonist (±)-SNAP-7941. Binding studies evinced high binding affinity of the non-radioactive derivatives. Small-animal imaging of [^{11}C]SNAP-7941 and [^{18}F]FE@SNAP evinced high tracer uptake in MCHR1-rich regions of the ventricular system. Quantitative analysis depicted a significant tracer reduction after displacement with (±)-SNAP-7941. Due to the high binding affinity of the non-labelled derivatives and the high specific tracer uptake of [^{11}C]SNAP-7941 and [^{18}F]FE@SNAP, there is strong evidence that both radiotracers may serve as highly suitable agents for specific MCHR1 imaging.

The melanin-concentrating hormone (MCH) is a cyclic polypeptide consisting of 19 amino acids, produced predominantly by neurons in the lateral hypothalamus, incerto-hypothalamic area and zona incerta with extensive projections throughout the brain[1]. Besides, MCH is also found in peripheral organs and tissues, such as the pancreas[2], colonic epithelial cells[3] or adipocytes[4,5]. The biological effects of MCH are mediated by two G-protein coupled receptors (GPCRs), termed MCH receptor 1 (MCHR1)[6–9] and MCH receptor 2 (MCHR2)[10–13]. While the MCHR1 has been isolated from rodents and humans[6,8], the MCHR2 has thus far been identified in primates, dogs, ferrets and humans[10,11]. Several lines of research evinced that MCH acts as an important mediator in the integrated regulation of energy homeostasis and body weight and is linked with diseases such as diabetes, insulin resistance, colitis and obesity[14–20]. The distribution of MCH and the expression of the MCHR1 in the brain outside of regions connected with nutritional behaviour, has led to the finding that MCH signalling is also involved in a

[1]Department of Biomedical Imaging and Image-guided Therapy, Division of Nuclear Medicine, Medical University of Vienna, Vienna, Austria. [2]Department of Engineering, University of Applied Sciences Wiener Neustadt, Wiener Neustadt, Austria. [3]Department of Biomedical Imaging and Image-guided Therapy, Division of Molecular and Gender Imaging, Medical University of Vienna, Vienna, Austria. [4]Department of Inorganic Chemistry, University of Vienna, Vienna, Austria. [5]CBmed GmbH, Center for Biomarker Research in Medicine, Graz, Austria. [6]Department of Organic Chemistry, University of Vienna, Vienna, Austria. [7]Department of Pharmaceutical Chemistry, University of Vienna, Vienna, Austria. [8]Department of Psychiatry and Psychotherapy, Medical University of Vienna, Vienna, Austria. [9]Department of Pharmaceutical Technology and Biopharmaceutics, University of Vienna, Vienna, Austria. [10]Ludwig Boltzmann Institute for Applied Diagnostics, Vienna, Austria. Correspondence and requests for materials should be addressed to M.M. (email: markus.mitterhauser@meduniwien.ac.at)
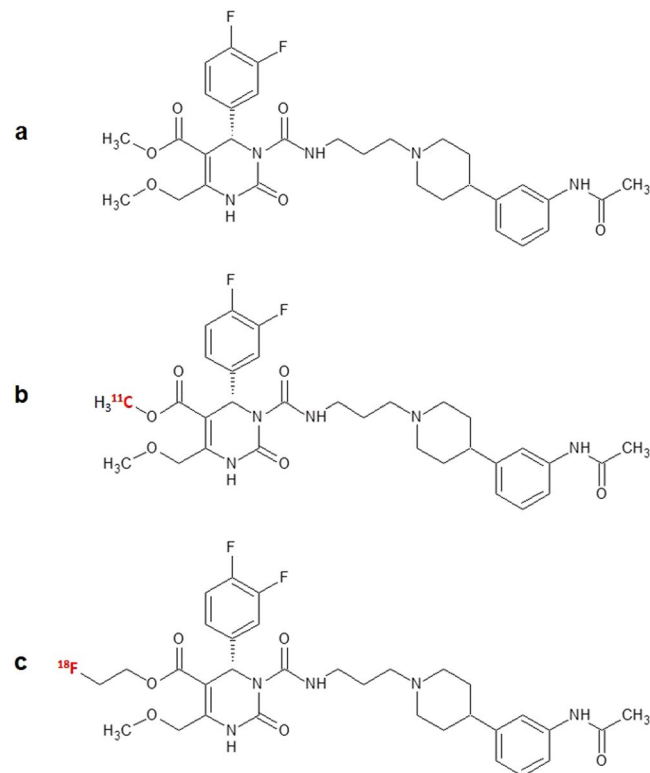
Figure 1. Chemical structures of the MCHR1 antagonists. Chemical Structures of (+)-SNAP-7941 (**a**), [11C]
SNAP-7941 (**b**) and [18F]FE@SNAP **(c)**. The red colored atom indicates the position of the radioisotope
introduced by radiolabeling.

variety of psychiatric disorders, such as depression and anxiety[21]. Previous studies have shown, that MCH acts
as an important mediator of cerebrospinal fluid (CSF) homeostasis and positively controls cilia beat frequency
of ependymal cells, whereas a lack of MCHR1 provokes an increase in ventricular size[22, 23]. Given the fact that
ependymal cells and MCH neurons are both involved in glucose sensing[24–26], MCH fibres could control the activ-
ity of ciliated cells to initiate an increase in CSF flow to meet metabolic needs. This strongly supports the idea that
the MCH-system may also be involved in non-neuronal intercellular communication, but evidence is still lacking.
However, to enable a quantitative *in vivo* assessment of the MCHR1 pharmacology and to facilitate preclinical
to clinical translation, a suitable positron emission tomography (PET) tracer needs to be developed. Based on
the specific MCHR1 antagonist (+)-methyl(4 S)-3-{[(3-{4-[3-(acetylamino)phenyl]-1piperidinyl}propyl)amino]
carbonyl}-4-(3,4-difluorophenyl)-6-(methoxymethyl)-2-oxo-1,2,3,4-tetra-hydro-5-pyrimidenecarboxylate
hydrochloride ((+)-SNAP-7941; Fig. 1a)[27], the successful preparation of the first potential PET radiotracers [11C]
SNAP-7941 (Fig. 1b) and the [18F]fluoroethylated analogue [18F]FE@SNAP (Fig. 1c) was performed[28, 29]. Since
both tracers yield adequate amounts of radioactivity with suitable molar activity, initial preclinical evaluation has
been accomplished[30, 31].

Based on the preceding results, the current study focused on the quantitative *in vitro* and *in vivo* assessment of
main biological and physicochemical properties of [18F]FE@SNAP and [11C]SNAP-7941 and the corresponding
non-radioactive derivatives to enable confidence about the MCHR1 pharmacology. In detail, the aims of the study
were (i) competitive binding studies with the non-radioactive derivatives, (ii) small-animal PET/CT and MRI
studies of healthy rats with MCHR1 displacement and (iii) small-animal PET/CT and MRI studies of healthy rats
under baseline conditions.

Results

Competitive binding studies. Displacement of specific [125I]MCH binding on CHO-K1 membranes,
expressing the hMCHR1, in presence of the different MCHR1 ligands evinced high binding affinity for (±)-
SNAP-7941 and (+)-SNAP-7941, both in a low nanomolar range, whereas the binding affinity of FE@SNAP was
determined to be significantly lower (Fig. 2 and Table 1). Differences of the K_i values between (±)-SNAP-7941and
(+)-SNAP-7941 were found to be statistically not significant ($P > 0.05$). MCH revealed high binding affinity with
a K_i in a low nanomolar range and was found to be in good agreement with previously reported values. Hill slope
factors of (±)-SNAP-7941, FE@SNAP and MCH indicated no binding cooperativity and were determined to be
statistically not significantly different ($P > 0.05$). On the contrary the Hill slope factor of (+)-SNAP-7941 was
found to be significantly higher and revealed a strong positive cooperativity. A detailed summary of correspond-
ing IC_{50}, K_i and Hill slope factors of the dedicated MCHR1 ligands is shown in Table 1.
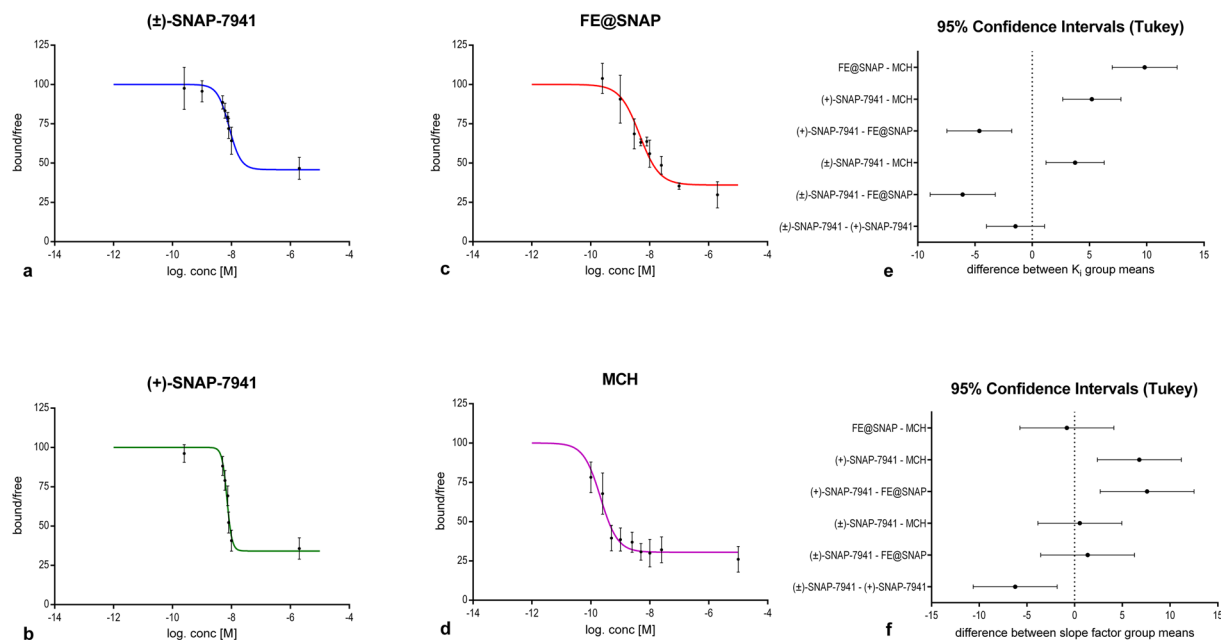
Figure 2. Competitive binding studies. Displacement of specific [^{125}I]MCH binding on CHO-K1 cell membranes expressing the hMCHR1 in presence of different concentrations of ($\pm$)-SNAP-7941 (**a**), ($+$)-SNAP-7941 (**b**), FE@SNAP (**c**) and MCH (**d**). Differences between group means of the K_i (**e**) and the dedicated Hill slope factor (**f**) with corresponding 95% confidence intervals. Data are plotted as mean $\pm$ SEM from three independent experiments each performed in quadruplicate. If not visible the error bars are within the margin of the symbols.

Compound	IC$_{50}$ [nM]	K_i [nM]	Hill slope factor
($\pm$)-SNAP-7941	5.61 ± 1.06	3.91 ± 0.74	2.66 ± 0.39
($+$)-SNAP-7941	7.70 ± 0.35	5.37 ± 0.25	8.89 ± 1.59
FE@SNAP	14.32 ± 1.61	9.98 ± 1.12	1.30 ± 0.33
MCH	0.24 ± 0.05	0.16 ± 0.03	2.11 ± 0.63

Table 1. Binding affinity of MCHR1 antagonists. Displacement of specific [^{125}I]MCH binding on CHO-K1 cell membranes expressing the hMCHR1. Data in the table are expressed as mean $\pm$ SEM from three independent experiments each performed in quadruplicate.

Small-animal imaging. Small-animal PET/MRI brain scans in healthy rats evinced high radiotracer uptake in the entire ventricular system for [^{11}C]SNAP-7941 and [^{18}F]FE@SNAP respectively, whereas the uptake in other brain regions was found to be comparable low. Representative triplanar PET/MRI rat brain scans are shown in Fig. 3 ([^{11}C]SNAP-7941) and Fig. 4 ([^{18}F]FE@SNAP). Differences between the mean SUV in the ventricular system before and after displacement with 15 mg/kg ($\pm$)-SNAP-7941 were found to be statistically significant for both [^{11}C]SNAP-7941 (Figs 3a and 5b) and [^{18}F]FE@SNAP (Figs 4a and 5d). As opposed to this no effect was determined after displacement of the basal radiotracer uptake with the vehicle for [^{11}C]SNAP-7941 (Figs 3b and 5a) and [^{18}F]FE@SNAP (Figs 4b and 5c). A detailed summary of all mean SUV values, of both radiolabelled compounds before and after displacement with ($\pm$)-SNAP-7941, the corresponding vehicle and corresponding P values are shown in Table 2. Whole brain uptake of [^{11}C]SNAP-7941 was found to be significantly reduced after displacement with ($\pm$)-SNAP-7941 (Fig. 6b), whereas in the group where the vehicle was used as displacement agent differences were proved to be statistically not significant (Fig. 6a). In contrast to that, differences of the whole brain uptake of [^{18}F]FE@SNAP before and after displacement were found to be statistically not significant for both displacement with ($\pm$)-SNAP-7941 (Fig. 6d) and the vehicle (Fig. 6c). Since the brains of all groups were counted in the Gamma Counter too, the findings of the micro PET scans could be confirmed. *Ex-vivo* brain uptake of [^{11}C]SNAP-7941 measured in the Gamma Counter revealed a normalized value (mean $\pm$ SEM, expressed as %ID/g) of 0.023 ± 0.002 for the vehicle group and 0.015 ± 0.002 for the group where displacement was introduced via ($\pm$)-SNAP-7941. Differences of group means were proven to be statistically significant ($P = 0.0156$). *Ex-vivo* brain uptake of [^{18}F]FE@SNAP revealed a normalized value (mean $\pm$ SEM, expressed as %ID/g) of 0.020 ± 0.001 for the vehicle group and 0.018 ± 0.003 for the group where displacement was introduced via ($\pm$)-SNAP-7941. No significant effect between both groups was observed ($P = 0.4547$). TACs of the whole brain and the ventricular system of [^{11}C]SNAP-7941 and [^{18}F]FE@SNAP before and after displacement with
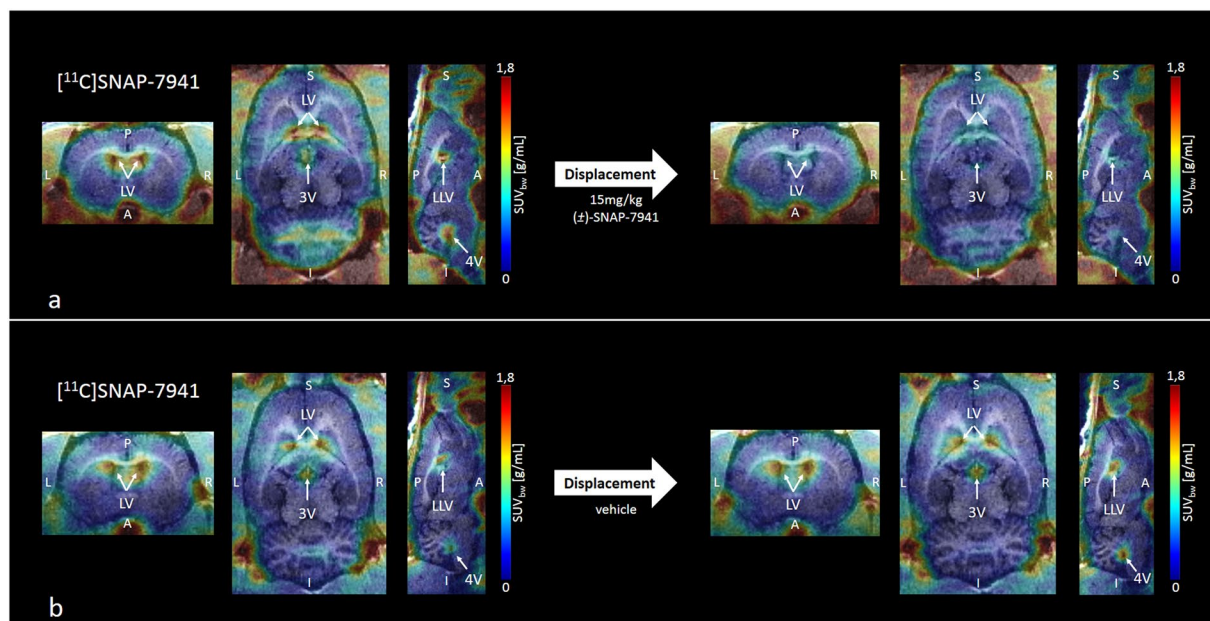
Figure 3. Small-animal PET/MR brain images of [^{11}C]SNAP-7941. Exemplary small-animal PET/MR images of representative coronal (left), horizontal (centre) and sagittal (right) planes of a rat brain with [^{11}C]SNAP-7941 before and after administration of 15 mg/kg ($\pm$)-SNAP-7941 (**a**) and with [^{11}C]SNAP-7941 before and after administration of the corresponding vehicle (**b**). PET data are contributed to summation images from 0–15 minutes (before displacement) and from 15–45 minutes (after displacement). Anatomical structures are indicated by arrows (**LV** = lateral ventricle; **LLV** = left lateral ventricle; **3V** = third ventricle; **4V** = fourth ventricle).
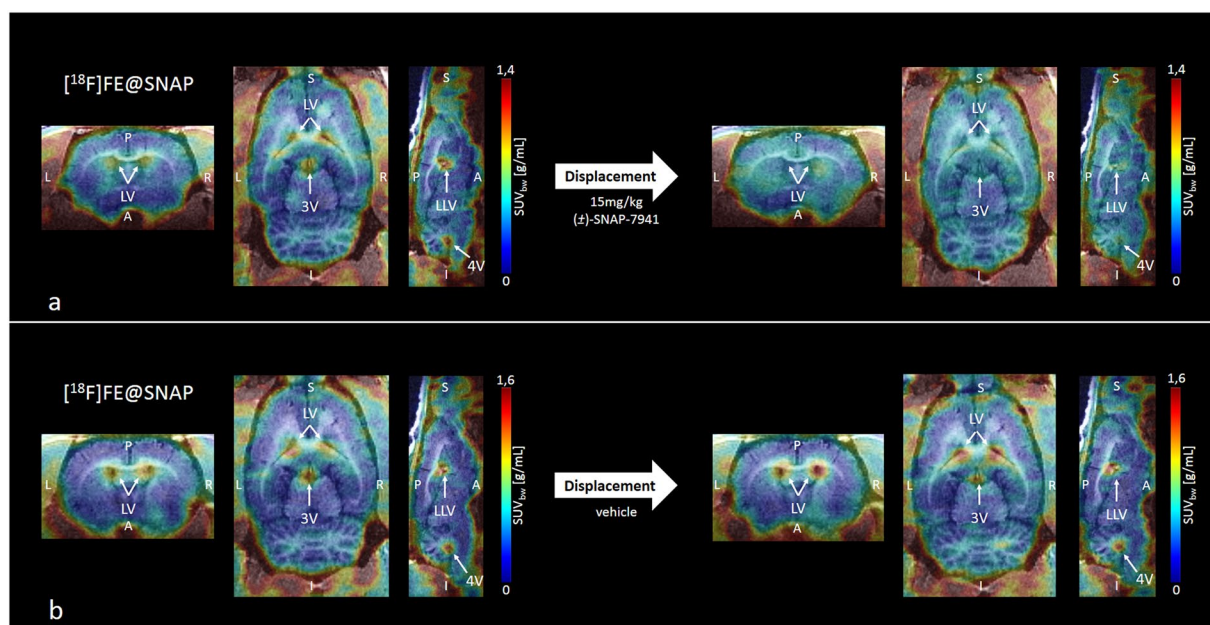
Figure 4. Small-animal PET/MR brain images of [^{18}F]FE@SNAP. Exemplary small-animal PET/MR images of representative coronal (left), horizontal (centre) and sagittal (right) planes of a rat brain with [^{18}F]FE@SNAP before and after administration of 15 mg/kg ($\pm$)-SNAP-7941 (**a**) and with [^{18}F]FE@SNAP before and after administration of the corresponding vehicle (**b**). PET data are contributed to summation images from 0–20 minutes (before displacement) and from 20–60 minutes (after displacement). Anatomical structures are indicated by arrows (**LV** = lateral ventricle; **LLV** = left lateral ventricle; **3V** = third ventricle; **4V** = fourth ventricle).
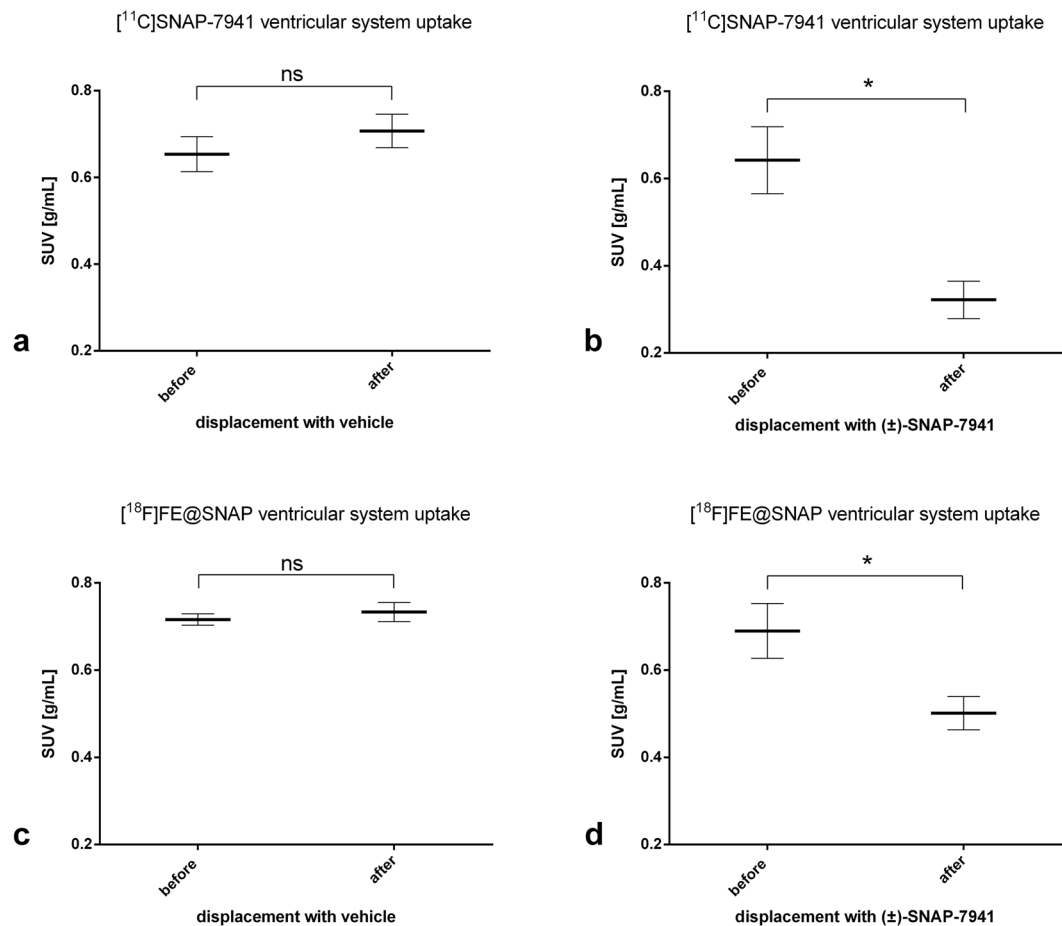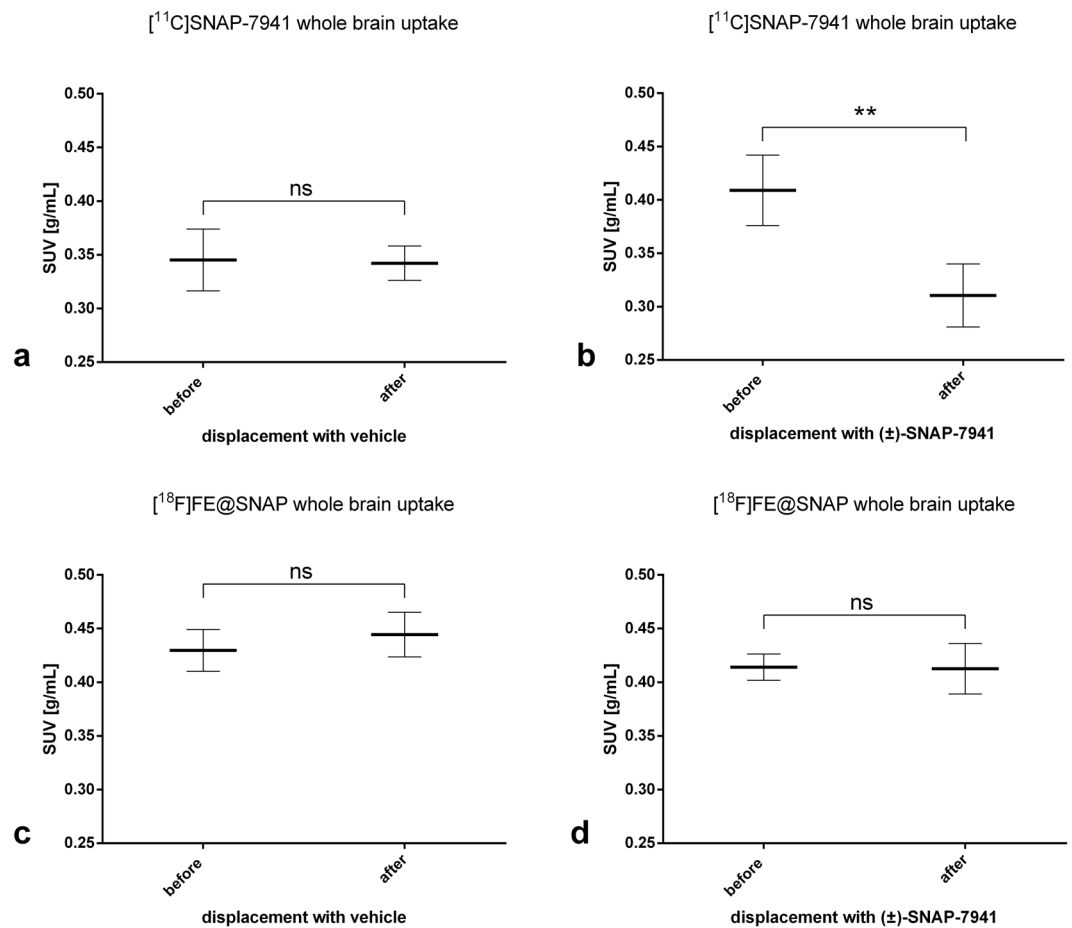
Figure 5. Radiotracer uptake in the ventricular system. Radiotracer uptake in the ventricular system of [11C] SNAP-7941 before and after displacement with either vehicle (**a**) or 15 mg/kg (±)-SNAP-7941 (**b**) and [18F]FE@ SNAP before and after displacement with either vehicle (**c**) or 15 mg/kg (±)-SNAP-7941 (**d**). Data are displayed as mean ± SEM from independent experiments (n ≥ 3). Differences among groups were tested using a two-tailed parametric paired t-test (ns = P > 0.05; *P < 0.05). If not visible, error bars are within the margin of the symbols.

[11C]SNAP-7941 displacement with (±)-SNAP-7941	SUV$_{bw}$ [g/mL]		
Region	*Baseline*	*Displacement*	*P value*
Whole brain	0.41 ± 0.03	0.31 ± 0.03	0.003
Ventricular system	0.64 ± 0.08	0.32 ± 0.04	0.012
[11C]SNAP-7941 displacement with vehicle	SUV$_{bw}$ [g/mL]		
Whole brain	0.35 ± 0.03	0.34 ± 0.02	0.845
Ventricular system	0.65 ± 0.04	0.71 ± 0.04	0.184
[18F]FE@SNAP displacement with (±)-SNAP-7941	SUV$_{bw}$ [g/mL]		
Whole brain	0.41 ± 0.01	0.41 ± 0.02	0.936
Ventricular system	0.69 ± 0.06	0.50 ± 0.04	0.022
[18F]FE@SNAP displacement with vehicle	SUV$_{bw}$ [g/mL]		
Whole brain	0.43 ± 0.02	0.44 ± 0.02	0.198
Ventricular system	0.72 ± 0.01	0.73 ± 0.02	0.292

Table 2. Radiotracer uptake in the whole brain and the ventricular system. SUV$_{bw}$ mean values for the radiotracer uptake in the whole brain and the ventricular system of [11C]SNAP-7941 and [18F]FE@SNAP, both before and after displacement with either 15 mg/kg (±)-SNAP-7941 or vehicle with corresponding P values. Data in the table are expressed as mean ± SEM from independent experiments (n ≥ 3). Differences between baseline and displacement conditions were tested using a two-tailed parametric paired t-test. Values of P < 0.05 were considered as statistically significant.

Figure 6. Radiotracer uptake in the whole brain. Whole brain uptake of [11C]SNAP-7941 before and after displacement with either vehicle (**a**) or 15 mg/kg ($\pm$)-SNAP-7941 (**b**) and [18F]FE@SNAP before and after displacement with either vehicle (**c**) or 15 mg/kg ($\pm$)-SNAP-7941 (**d**). Data are displayed as mean $\pm$ SEM from independent experiments (n $\geq$ 3). Differences among groups were tested using a two-tailed parametric paired t-test (ns $=$ P $>$ 0.05; **P $<$ 0.01). If not visible, error bars are within the margin of the symbols.

either the vehicle compound or with ($\pm$)-SNAP-7941 are shown in Fig. 7. [11C]SNAP-7941 displayed fast tracer equilibrium and a stable signal over the whole time course of the experiment for the group where the vehicle was used for displacement (Fig. 7a and c, blue line with triangles), whereas a clear drop in the TACs for both, whole brain and the ventricular system, was observed after displacement with 15 mg/kg ($\pm$)-SNAP-7941 (Fig. 7a and c, red line with circles). TACs of [18F]FE@SNAP evinced fast tracer equilibrium and a stable signal over the whole course of investigation for the whole brain and the ventricular system in the group where displacement was introduced via the vehicle (Fig. 7b and d, blue line with triangles). A clear drop of the TAC of [18F]FE@SNAP was shown immediately after displacement with 15 mg/kg ($\pm$)-SNAP-7941 (Fig. 7d, red line with circles), whereas no differences in the TAC of the whole brain was observed after treating the animals with the respective antagonist (Fig. 7c, red line with circles).

Discussion

The *in vivo* quantification of MCHR1 pharmacology is a crucial step for the better understanding of the pathogenesis of a variety of endocrine disorders like obesity, diabetes and insulin resistance. Therefore a specific PET radiotracer for MCHR1 imaging is of high scientific interest, since it comprises several advantages for clinical medicine and biomedical research, such as monitoring of the hormone receptor status and related pathologies *in-vivo*, compound dose selection and the *in vivo* quantification of the MCHR1 as a risk factor and early diagnostic tool for adiposity, diabetes and insulin resistance. To foster the *in-vivo* imaging of the MCHR1, PET radiotracer development was initiated[28–33]. Based on the preceding results, the current study focused on the quantitative *in vitro* and *in vivo* assessment of main biological and physicochemical properties of [18F]FE@SNAP and [11C]SNAP-7941 and corresponding non-radioactive derivatives to enable confidence about the MCHR1 pharmacology. Due to the low density of the MCHR1 in the human brain ($B_{Max} = 5.8 \pm 0.3$ fmol/mg)[34], a high binding affinity is mandatory. In the present paper we demonstrated high binding affinity in a low nanomolar range for our non-labeled reference compounds FE@SNAP, ($\pm$)-SNAP-7941 and ($+$)-SNAP-7941 in competition experiments using CHO-K1 cell membranes expressing the hMCHR1. Although no significant difference of the Ki of ($\pm$)-SNAP-7941 and ($+$)-SNAP-7941 was found, the Hill slope factor of ($+$)-SNAP-7941 was significantly
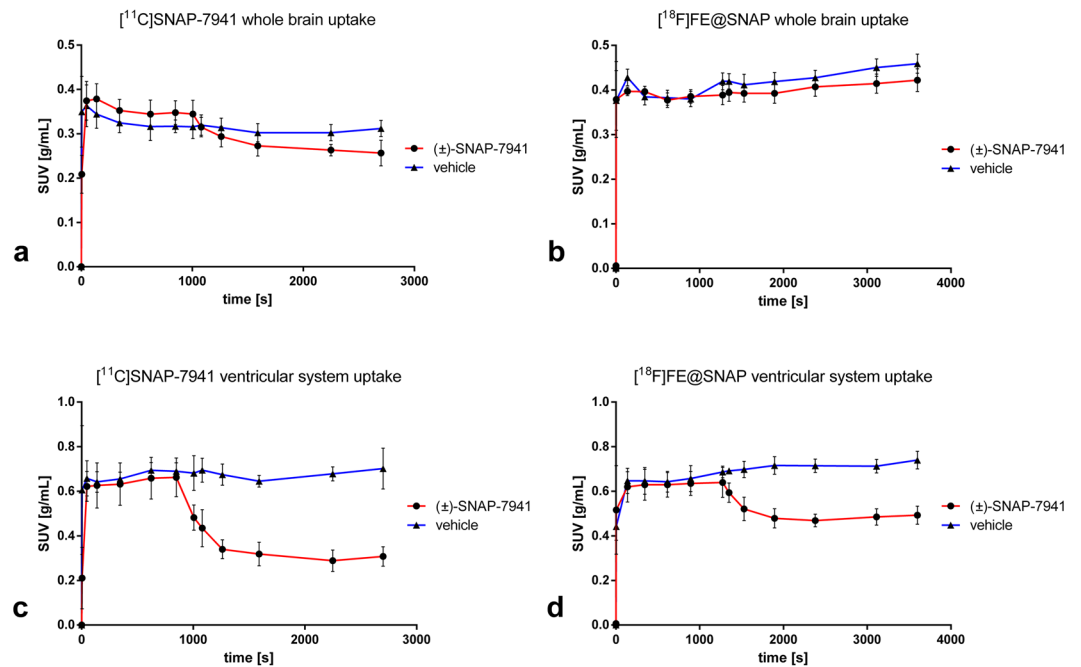
Figure 7. Time–activity curves of [11C]SNAP-7941 and [18F]FE@SNAP. Time–activity curves (mean SUV ± SEM) indicating the whole brain uptake of [11C]SNAP-7941 (**a**) and [18F]FE@SNAP (**b**) and the uptake in the ventricular system of [11C]SNAP-7941 (**c**) and [18F]FE@SNAP (**d**). Curves depict basal tracer kinetics followed by displacement with either 15 mg/kg (±)-SNAP-7941 (red line with circles) or the vehicle (blue line with triangles). Data are expressed as mean ± SEM from three independent experiments. If not visible, error bars are within the margin of the symbols.

higher, indicating a strong positive cooperativity. Potential advantages and physiological cross-influences due to high positive binding cooperativity for the *in vivo* assessment of the MCHR1 pharmacology still remain unclear and need to be evaluated in future imaging studies. However, FE@SNAP and (±)-SNAP-7941 evinced no binding cooperativity and compared to the natural hormone MCH, differences were proved to be statistically not significant. It has been described that the MCHR1 is expressed in central brain regions, like the lateral hypothalamus, inceto-hypothalamic area and the zona incerta[1], but recent studies revealed also a high level of MCHR1 expression in the ependymal cells of the ventricular system[22]. Since there is still a lack of potential imaging biomarkers targeting the MCHR1, the study focused on the potential of [11C]SNAP-7941 and [18F]FE@SNAP to specifically label MCHR1-rich regions in healthy rats under baseline and displacement conditions. Intravenous injection of [11C]SNAP-7941 and [18F]FE@SNAP evinced high tracer uptake in the ventricular system (see Figs 3 and 4), which supports the expression of the MCHR1 in the ventricular system as reported in previous studies[22, 23]. Further quantitative analysis depicted a clear and statistically significant reduction of the tracer uptake for both [11C]SNAP-7941 and [18F]FE@SNAP after displacement with (±)-SNAP-7941, whereas displacement with the vehicle revealed no effect (Fig. 5), indicating high specific radiotracer uptake on MCHR1-rich regions on the ependymal cells of the ventricular system. Compared to the uptake in the ventricular system, whole brain uptake was rather low for both [11C]SNAP-7941 and [18F]FE@SNAP. Detailed quantitative analysis of the whole brain uptake of [18F]FE@SNAP before and after displacement with (±)-SNAP-7941 revealed no significant difference. Interestingly, we found a significant difference in the whole brain uptake before and after displacement with (±)-SNAP-7941 for [11C]SNAP-7941 (Fig. 6). The result may be biased due to the higher specific uptake in the ventricular system of [11C]SNAP-7941 and the fast metabolism of [18F]FE@SNAP[30]. Knowing from initial preclinical experiments with [11C]SNAP-7941[31], the low uptake in MCHR1 rich regions in the brain may be caused by limited blood-brain-barrier penetration due to binding to P-glycoprotein (P-gp) and Breast Cancer Resistance Protein (BCRP).

Since the MCHR1 is highly expressed in the ependymal cells of the epithelium of the ventricular system, a tracer for the MCHR1 should show specific uptake and be significantly reduced by an unlabeled ligand in these areas. The specificity of [11C]SNAP-7941 and [18F]FE@SNAP was successfully proven in small animal PET studies by displacement with the unlabeled MCHR1 antagonist (±)-SNAP-7941, which confirmed that both radiotracers are highly specific agents for MCHR1 imaging. Further, these results were affirmed by *ex vivo* brain autoradiography in a previous study[32]. Since the MCHR1 is primarily involved in the integrated regulation of energy homeostasis, [11C]SNAP-7941 and [18F]FE@SNAP may serve as a useful tool for imaging and therapy monitoring of a broad range of connected disease such as diabetes, adiposity and insulin resistance. Given the fact that ependymal cells and MCH neurons are both involved in glucose sensing[24–26] MCH fibres could control the activity of ciliated cells to initiate an increase in CSF flow to meet metabolic needs. Therefore both [11C]SNAP-7941 and [18F]FE@SNAP may serve a high potential candidates to investigate the involvement of the MCH-system in non-neuronal

intercellular communication. Future small animal experiments will focus on the global pharmacodynamics and –kinetics of both radiotracers addressing the peripheral involvement of MCHR1. These insights should facilitate the monitoring and treatment of MCHR1 related pathologies.

Methods

Radioligands and chemical compounds. The radioionated no carrier added (n.c.a.) MCHR1 agonist [125I]-Tyr[13]-melanin-concentrating hormone ([125I]MCH) was purchased from PerkinElmer® (PerkinElmer, Inc., Waltham, MA, USA). The radioligand [125I]MCH was described to reveal high affinity towards the MCHR1[13, 35] and used to serve as a radiolabelled reference compound for the competitive binding experiments.

The non-radioactive reference compound MCH was purchased from Sigma-Aldrich® (Sigma-Aldrich, St. Louis, MO, USA). The MCHR1 antagonists including the racemic mixture of SNAP-7941 ((±)-SNAP-7941), the enantiomeric form (+)-SNAP-7941 and the fluoroethylated analogue (+)-(2-Fluoroethyl)(4 S)-3-{[(3-{4-[3-(acetylamino)phenyl]-1-piperidinyl}propyl)amin]carbonyl}-4-(3,4-difluorophenyl)-6-(methoxymethyl)-2-oxo-1,2,3,4-tetra-hydro-5-pyrimidenecarboxylate (FE@SNAP), as well as the precursor compounds (4S)-3-{[(3-{4-[3-(acetylamino)phenyl]-1piperidinyl}propyl)amino]carbonyl}-4-(3,4-difluorophenyl)-6-(methoxymethyl)-2-oxo-1,2,3,4-tetra-hydro-5-pyrimidenecarboxylate acid (SNAP-acid) and 2-(Tosyloxy)ethyl-3-{[(3-{4-[3-(acetylamino)phenyl]-1piperidinyl}propyl)amino]carbonyl}-4-(3,4-difluorophenyl)-6-(methoxy-ethyl)-2-oxo-1,2,3,4-tetra-hydro-5-pyrimidenecarboxylate acid (Tos@SNAP) were synthesized in collaboration with the Department of Pharmaceutical Chemistry and the Department Organic Chemistry of the University of Vienna (Vienna, Austria) as previously reported[36, 37]. All other chemicals were of analytical grade and purchased from commercial sources.

Tracer preparation. Radiosynthesis of [11C]SNAP-7941, the radiolabeled analogue of (±)-SNAP-7941, was performed in a fully automated synthesizer (TRACERlab™ FX C Pro, GE Healthcare, Germany) as previously reported[28]. Radiosynthesis of [18F]FE@SNAP was performed in a microfluidic device (Advion NanoTek®, Ithaca, NY, USA) as described elsewhere[29, 30], followed by a purification in a conventional synthesizer unit (Nuclear Interface®, GE Medical Systems, Uppsala, Sweden). Both radiotracers are formulated in physiological saline solution for intravenous injection. Radiochemical purity and molar activity of [11C]SNAP-7941 and [18F]FE@SNAP were determined by analytical radio-HPLC (Agilent, Boeblingen, Germany).

Competitive binding studies. Competitive binding studies were conducted on CHO-K1 cell membranes expressing the hMCHR1 (PerkinElmer, Inc., Waltham, USA). Briefly, cell membranes (10 μg/mL) were dissolved in 500 μL 50 mM Tris buffer (pH 7.4) (containing 10 mM $MgCl_2$, 2 mM EDTA, 0.1% bacitracin and 0.2% BSA). The equilibrium inhibition constant (K_i) was evaluated using several concentrations (0.1–10 000 nM) of MCH, (±)-SNAP-7941, (+)-SNAP-7941 and FE@SNAP in the presence of 0.1 nM [125I]MCH. All non-labelled compounds were initially dissolved in DMSO and diluted with deionized water to the final concentration, where the amount of DMSO never exceeded 5%. The membranes were incubated in vials at room temperature for 120 min. Subsequently, bound and free fractions of radioligand were separated by centrifugation at $40\,000 \times g$ for 20 min. The supernatants were removed into new vials and pellets were washed twice with 800 μL ice cold Tris buffer. The pellets were finally dissolved in 1300 μL Tris buffer and the radioactivity of both, the supernatant and the pellet, was measured in a Gamma Counter (2480 WIZARD^2, PerkinElmer, Waltham, MA, USA). The half-maximum inhibitory concentration (IC_{50}) was determined using GraphPad Prism 6.0 (GraphPad Software, Inc., San Diego, CA, USA) and converted into the K_i using the Cheng Prusoff equation[38].

Animals. Twelve-weeks old male Sprague-Dawley rats (HIM:OFA, Himberg, Austria) weighing 389 ± 86 g were kept under controlled environmental conditions (22 ± 1 °C; 40–70% humidity; 12 hours light/dark cycle) with free access to water and standard laboratory animal diet (sniff R/M-H, sniff Spezialdiaeten GmbH, Soest, Germany). Prior to each experiment, the animals were placed into an induction chamber and anesthetized with 2.5% isoflurane. When unconscious, the animals were taken from the chamber and kept under anesthesia with 1.5–2.5% isoflurane provided via a mask during the whole experiment. Physiological parameters and the depth of anesthesia were monitored continuously. Administration of radioligands and MCHR1 antagonists were performed intravenously via the lateral tail vein. All procedures and protocols using animals have been approved by the Institutional Animal Care and Use Committee of the Medical University of Vienna, Austria, as well as by the Austrian Ministry of Science, Research and Economy (BMWFW-66.009/0029-WF/V/3b/2015). Every effort was made to minimize both, the suffering and the number of animals. All experimental procedures and protocols used in this study were performed in accordance with the relevant guidelines and regulations.

Small-animal imaging. Anaesthetized rats were immobilized in a multimodal animal carrier unit (MACU; medres® – medical research GmbH, Cologne, Germany) and maintained at a body temperature of 37 °C throughout the whole experiment. Animals received either [11C]SNAP-7941 or [18F]FE@SNAP, followed by an injection of (±)-SNAP-7941 (15 mg/kg body weight, freshly dissolved in 400 μL; displacement condition; n = 3) or 400 μL of the respective solvent (vehicle condition; n = 3). The MCHR1 antagonists and the vehicle were administered either 15 min ([11C]SNAP-7941) or 20 min ([18F]FE@SNAP) after radiotracer injection as a bolus via the lateral tail vein. A stereotactic holder attached to the MACU was used to fix the head of the animals in a reliable and reproducible position within the whole imaging study. Experiments were initiated with a 7 minute cone beam attenuation CT (CBCT) of the brain (360 projections; binning 4 × 4; 80 kV; 500 μA; 200 ms exposure time) using a small-animal CT scanner (Siemens Inveon microSPECT/CT, Siemens Medical Solutions, Knoxville, USA). Subsequently the animals were positioned in the imaging chamber of a Siemens Inveon micro-PET scanner (Siemens Medical Solution, Knoxville, USA). [11C]SNAP-7941 (75.85 ± 5.80 MBq; molar activity: 33.12 ± 25.73 GBq/μmol; radiochemical purity: >99%) or [18F]FE@SNAP (44.12 ± 4.41 MBq; molar activity:

22.18 ± 9.72 GBq/µmol; radiochemical purity: >90%) was injected (200–800 µL) via the lateral tail vein and dynamic PET imaging was performed 45 min for the [11C]-labeled radiotracer and 60 min for the [18F]-labeled ligand. Immediately afterwards, T1-weighted high-resolution axial, coronary and sagittal brain MRI scans (2D FLASH; echo time: 3.85 ms; repetition time: 282 ms; flip angle: 30°; field of view: 35 × 35 mm; resolution: 68 × 68 µm; slice thickness: 0.4 mm) were performed using a Bruker BioSpec 94/30 USR small-animal MR system (Bruker BioSpin GmbH, Karlsruhe, Germany). At the end of the imaging study animals were sacrificed under anesthesia through an intravenous injection of pentobarbital sodium (Release® 300 mg/mL, WDT, Garbsen, Germany), brains were removed, weighed and subjected to radioactivity measurements in a Gamma Counter (2480 WIZARD[2], PerkinElmer, Waltham, MA, USA). Values were normalized to weight and dose and expressed as the percentage injected dose per gram of tissue (%ID/g).

Image reconstruction and data post processing. CT raw data was reconstructed with a Feldkamp algorithm using a Shepp-Logan filter followed by standard rat beam-hardening correction and noise reduction (matrix size: 1024 × 1024; effective pixel size: 97.56 µm). PET list mode data was sorted into three-dimensional sinograms according to the following frame sequences, for [11C]SNAP-7941: 1 × 3 s, 3 × 2 s, 1 × 6 s, 1 × 15 s, 1 × 35 s, 1 × 145 s, 1 × 270 s, 1 × 285 s, 1 × 165 s, 3 × 30 s, 1 × 120 s, 1 × 240 s, 1 × 420 s, 1 × 900 s and for [18F] FE@ SNAP: 1 × 3 s, 3 × 2 s, 1 × 6 s, 1 × 15 s, 1 × 35 s, 1 × 145 s, 2 × 270 s, 1 × 285 s, 1 × 165 s, 3 × 30 s, 1 × 120 s, 1 × 240 s, 2 × 487 s, 1 × 976 s. PET images were reconstructed using an OSEM 3D/OP-MAP scatter corrected reconstruction algorithm and a ramp filter (matrix size 128 × 128). The data was normalized and corrected for random, dead time and radioactive decay. A calibration factor was applied to the data for converting units of the microPET images into absolute radioactivity concentration units.

Multimodal (microPET/CT/MRI) rigid-body image registration and biomedical image quantification was performed using the image analysis software PMOD 3.8 (PMOD Technologies Ltd, Zurich, Switzerland) and Inveon Research Workplace (IRW; Siemens Medical Solutions, Knoxville, USA). Volumes of interest (VOIs), comprising the whole brain and the ventricular system of the rats, were outlined on multiple planes of the CT and MRI images and transferred to the PET images of the individual time frames. Time–activity curves (TACs) were calculated, normalized to dose and weight and expressed as standardized uptake values (SUV; g/mL) to facilitate comparison.

Statistical analysis. Unless mentioned otherwise all experimental data are expressed as mean ± SEM from at least three independent experiments with different batches of radioligand. Statistical testing was performed using GraphPad Prism 6 (GraphPad Software, Inc., San Diego, CA). Descriptive statistical measures were used to confirm the goodness of the nonlinear regression models. Differences among groups and conditions were proved using either a two tailed, unpaired Student's *t*-test with Welch's correction or a two-tailed parametric paired *t*-test. Multiple comparisons testing were performed using either ordinary one-way ANOVA with Tukey's correction or ordinary two-way ANOVA with Sidak's correction. Values of $P < 0.05$ were considered as statistically significant.

References

1. Bittencourt, J. C. Anatomical organization of the melanin-concentrating hormone peptide family in the mammalian brain. *Gen Comp Endocrinol* **172**, 185–197 (2011).
2. Tadayyon, M., Welters, H. J., Haynes, A. C., Cluderay, J. E. & Hervieu, G. Expression of melanin-concentrating hormone in insulin-producing cells: MCH stimulates insulin release in RINm5F and CRI-G1 cell-lines. *Biochem Biophys Res Commun* **275**, 709–712 (2000).
3. Kokkotou, E. *et al*. Melanin-concentrating hormone as a mediator of intestinal inflammation. *Proc Natl Acad Sci USA* **105**, 10613–10618 (2008).
4. Bradley, R. L., Kokkotou, E. G., Maratos-Flier, E. & Cheatham, B. Melanin-concentrating hormone regulates leptin synthesis and secretion in rat adipocytes. *Diabetes* **49**, 1073–1077 (2000).
5. Bradley, R. L., Mansfield, J. P., Maratos-Flier, E. & Cheatham, B. Melanin-concentrating hormone activates signaling pathways in 3T3-L1 adipocytes. *Am J Physiol Endocrinol Metab* **283**, 584–592 (2002).
6. Saito, Y. *et al*. Molecular characterization of the melanin-concentrating-hormone receptor. *Nature* **400**, 265–269 (1999).
7. Shimomura, Y. *et al*. Isolation and identification of melanin-concentrating hormone as the endogenous ligand of the SLC-1 receptor. *Biochem Biophys Res Commun* **261**, 622–626 (1999).
8. Chambers, J. *et al*. Melanin-concentrating hormone is the cognate ligand for the orphan G-protein-coupled receptor SLC-1. *Nature* **400**, 261–265 (1999).
9. Lembo, P. M. *et al*. The receptor for the orexigenic peptide melanin-concentrating hormone is a G-protein-coupled receptor. *Nat Cell Biol* **1**, 267–271 (1999).
10. Sailer, A. W. *et al*. Identification and characterization of a second melanin-concentrating hormone receptor, MCH-2R. *Proc Natl Acad Sci USA* **98**, 7564–7569 (2001).
11. Hill, J. *et al*. Molecular cloning and functional characterization of MCH2, a novel human MCH receptor. *J Biol Chem* **276**, 20125–20129 (2001).
12. Wang, S. *et al*. Identification and pharmacological characterization of a novel human melanin-concentrating hormone receptor, MCH-R2. *J Biol Chem* **276**, 34664–34670 (2001).
13. An, S. *et al*. Identification and characterization of a melanin-concentrating hormone receptor. *Proc Natl Acad Sci USA* **98**, 7576–7581 (2001).
14. Casatti, C. A. *et al*. Distribution of melanin-concentrating hormone neurons projecting to the medial mammillary nucleus. *Neuroscience* **115**, 899–915 (2002).
15. Marsh, D. J. *et al*. Melanin-concentrating hormone 1 receptor-deficient mice are lean, hyperactive, and hyperphagic and have altered metabolism. *Proc Natl Acad Sci USA* **99**, 3240–3245 (2002).
16. Ito, M. *et al*. Characterization of MCH-mediated obesity in mice. *Am J Physiol Endocrinol Metab* **284**, 940–945 (2003).
17. Ito, M. *et al*. Melanin-concentrating hormone 1-receptor antagonist suppresses body weight gain correlated with high receptor occupancy levels in diet-induced obesity mice. *Eur J Pharmacol* **624**, 77–83 (2009).
18. Elliott, J. C. *et al*. Increases in melanin-concentrating hormone and MCH receptor levels in the hypothalamus of dietary-obese rats. *Mol Brain Res* **128**, 150–159 (2004).

19. Schwartz, M. W., Woods, S. C., Porte, D. Jr., Seeley, R. J. & Baskin, D. G. Central nervous system control of food intake. *Nature* **404**, 661–671 (2000).
20. Pereira-da-Silva, M., De Souza, C. T., Gasparetti, A. L., Saad, M. J. & Velloso, L. A. Melanin- concentrating hormone induces insulin resistance through a mechanism independent of body weight gain. *J Endocrinol* **186**, 193–201 (2005).
21. Smith, D. G. *et al.* Melanin-concentrating hormone-1 receptor modulates neuroendocrine, behavioral, and corticolimbic neurochemical stress responses in mice. *Neuropsychopharmacology* **31**, 1135–1145 (2006).
22. Conductier, G. *et al.* Melanin-concentrating hormone regulates beat frequency of ependymal cilia and ventricular volume. *Nat Neurosci* **16**, 845–847 (2013).
23. Conductier, G. *et al.* Control of ventricular ciliary beating by the melanin concentrating hormone-expressing neurons of the lateral hypothalamus: a functional imaging survey. *Front Endocrinol* **182** (2013).
24. García, M. *et al.* Hypothalamic ependymal-glial cells express the glucose transporter GLUT2, a protein involved in glucose sensing. *J Neurochem* **86**, 709–724 (2003).
25. Psarra, A. M. *et al.* Immunocytochemical localization of glycogen phosphorylase kinase in rat brain sections and in glial and neuronal primary cultures. *J Neurocytol* **27**, 779–790 (1998).
26. Guyon, A. *et al.* Glucose inhibition persists in hypothalamic neurons lacking tandem-pore K+ channels. *J Neurosci* **29**, 2528–2533 (2009).
27. Borowsky, B. *et al.* Antidepressant, anxiolytic and anorectic effects of melanin-concentrating hormone-1 receptor antagonist. *Nat Med* **8**, 825–830 (2002).
28. Philippe, C. *et al.* Radiosynthesis of [11C]SNAP-7941-the first PET-tracer for the melanin concentrating hormone receptor 1 (MCHR1). *Appl Radiat Isotop* **70**, 2287–2294 (2012).
29. Philippe, C. *et al.* [18F]FE@SNAP-A new PET tracer for the melanin concentrating hormone receptor 1 (MCHR1): microfluidic and vessel-based approaches. *Bioorg Med Chem* **20**, 5936–5940 (2012).
30. Philippe, C. *et al.* Preparation and first preclinical evaluation of [18F]FE@SNAP: a potential PET tracer for the melanin concentrating hormone receptor 1 (MCHR1). *Sci Pharm* **81**, 625–639 (2013).
31. Philippe, C. *et al.* Preclinical *in vitro* & *in vivo* evaluation of [11C]SNAP-7941 - the first PET tracer for the melanin concentrating hormone receptor 1. *Nucl Med Biol* **40**, 919–925 (2013).
32. Philippe, C. *et al.* [(18)F]FE@SNAP-a specific PET tracer for melanin-concentrating hormone receptor 1 imaging? *EJNMMI Res* **31**, doi:10.1186/s13550-016-0186-7 (2016).
33. Igawa, H. *et al.* Development of a Novel Carbon-11 Labeled PET Radioligand for Melanin-Concentrating Hormone Receptor 1. *Curr Radiopharm* (2016).
34. Sone, M. *et al.* Binding sites for the melanin-concentrating hormone in the human brain. *Peptides* **21**, 245–250 (2000).
35. Audinot, V. *et al.* [125I]-S36057: a new and highly potent radioligand for the melanin-concentrating hormone receptor. *Br J Pharmacol* **133**, 371–378 (2001).
36. Schirmer, E. *et al.* Syntheses of precursors and reference compounds of the melanin-concentrating hormone receptor 1 (MCHR1) tracers [11C]SNAP-7941 and [18F]FE@SNAP for positron emission tomography. *Molecules* **18**, 12119–12143 (2013).
37. Goss, J. M. & Schaus, S. E. Enantioselective synthesis of SNAP-7941: chiral dihydropyrimidone inhibitor of MCH1-R. *J Org Chem* **73**, 7651–7656 (2008).
38. Cheng, Y. & Prusoff, W. H. Relationship between the inhibition constant (K1) and the concentration of inhibitor which causes 50 per cent inhibition (I50) of an enzymatic reaction. *Biochem Pharmacol* **22**, 3099–3108 (1973).

Acknowledgements

Author Contributions

M.Z., M.D., L.B. and F.P. performed the research, M.Z., C.P. and M.M. designed the research study, K.P., H.S., M.M., W.W., R.L. and M.H. contributed essential reagents and tools. M.Z., M.D. and F.P. analyzed the data. M.Z., C.P., M.D., F.P., R.L., W.W. and M.M. wrote the manuscript.

Additional Information

Competing Interests: This research was part of study funded by the Austrian Science Fund (FWF P20977-B09; P.I.: Markus Mitterhauser). No potential conflict of interest relevant to this article was reported.

Publisher's note: Springer Nature remains neutral with regard to jurisdictional claims in published maps and institutional affiliations.